THE JOURNAL OF PHYSICAL CHEMISTRY A

Article

pubs.acs.org/JPCA

# State-Selective Excitation of the CO Stretch in Carboxyhemoglobin by Mid-IR Laser Pulse Shaping: A Theoretical Investigation

Arunangshu Debnath,[†] Cyril Falvo,*[,‡] and Christoph Meier*[,†]

[†]LCAR-IRSAMC, Université Paul Sabatier, 31062 Toulouse, France

[‡]Institut des Sciences Moléculaires d'Orsay, UMR CNRS 8214, Univ Paris-Sud, 91405 Orsay, France

**ABSTRACT:** We present simulations of the excitation of specific vibrational levels of the CO stretch in carboxyhemoglobin by shaped mid-IR laser pulses. The pulses are calculated using local control theory, adapted to account for the protein fluctuations, which are included using a microscopic model developed previously. We show that efficient selective vibrational state preparation can be obtained, despite the presence of the fluctuations and orientational averaging, and can be monitored using transient absorption spectra. The mid-IR pulses are found to be in a realistic intensity regime and might soon be available by IR pulse shaping. This opens the way to a direct monitoring of vibrational relaxation from individually prepared, high-lying vibrational states of complex systems.

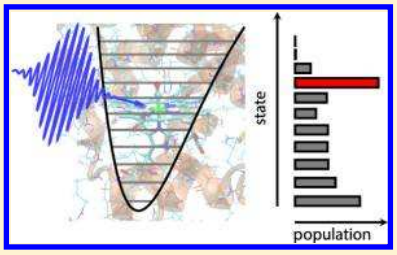


## INTRODUCTION

With the development of femtosecond laser technology, the study of ultrafast real-time dynamics in complex molecular systems, in particular, in the condensed phase, has become possible and yielded a detailed view of the underlying elementary processes.[1−4] Furthermore, with the development of pulse shaping devices, it is now possible not only to probe the quantum dynamics using laser fields but also to control its temporal evolution.[5−10] Recently, new pulse shaping devices operating directly in the infrared (IR) domain have been developed[11−14] and therefore allow shaped IR pulses at high intensities. This achievement paves the way to controlling molecular dynamics (MD) in the electronic ground state because at these wavelengths, the light pulses directly address the vibrations, an important aspect especially for complex systems such as proteins. While vibrational ladder climbing using chirped laser pulses (pulses with a linearly varying instantaneous frequency) was achieved several years ago both in isolated systems[15−21] as well as in carboxyhemoglobin (HbCO),[22] the excitation of individual, high-lying quantum states in complex systems is still a challenge. Because exciting specific modes to such high-lying states implies driving the system far out of equilibrium, their lifetimes are very sensitive to the protein environment. Several experimental measurements of relaxation times of high-lying excitations in complex systems have been reported,[11,12,17,22,23] and the leading experimentalists agree that the main obstacle in determining reliable vibrational lifetimes is the broad distribution of initial states, as typically obtained by vibrational ladder climbing using chirped laser pulses. Excitation of single quantum states would drastically enhance the results because the decay of the population can be directly monitored, without repopulation of decaying higher-lying states.[11,22]

This article presents a theoretical modeling of vibrational excitations of the CO stretch mode in HbCO to specific, predefined vibrational levels by suitably shaped mid-IR laser pulses. It is shown that the population of individual levels can be achieved to a high degree, even for an unoriented sample and under the influence of the protein environment, and both of these detrimental aspects are analyzed in detail. Furthermore, we calculate transient absorption spectra, taking experimental considerations like the effect of the spatial profile into account, and show that the created populations can be clearly measured by a weak probe pulse following the strong control pulse. As a consequence, by varying the time delay of the probe, a direct measurement of the decay of individual quantum states should be possible.

## THEORETICAL MODEL

Similar to the widely studied carboxymyogloboin (MbCO), the CO stretch band in HbCO has distinct subbands, reflecting different orientations and protonation states of the distal histidine.[24−29] However, in contrast to MbCO, in HbCO, the CO stretch is dominated by one band, termed the CIII band.[28,29] In the presented work, we have considered only one heme-CO site and an $N_\epsilon$ protonation of the distal histidine (Figure 1). While classical simulations can give reliable results on energy transfer in proteins,[30,31] in our case, a quantum treatment of the CO stretch is necessary, to account for the desired quantum state selectivity. However, for systems as large as proteins, or even one single active site, a full quantum treatment is out of reach. As a consequence, our approach is based on a one-dimensional (1D) parametrized quantum Hamiltonian. The full description of the model can be found in ref 32; however, we will briefly describe the main features of the model here. The parametrization is based on 500 random

**Received:** October 23, 2013
**Revised:** October 31, 2013
**Published:** November 1, 2013

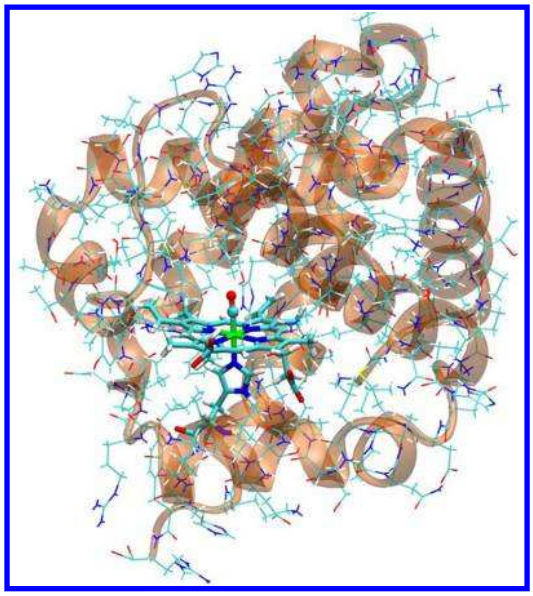

**Figure 1.** Protein structure used for the simulations.

snapshots of the active site embedded in the protein taken randomly from an equilibrium classical MD simulation. For each snapshot, a 1D cut along the CO stretch coordinate $q_0$ of the Fe(P)Im−CO complex was calculated using DFT using the B3LYP functional as implemented in Gaussian03,[33] treating the effect of the protein through point charges. The iron center is described by the Stuttgart effective core potential,[34] and the atoms of the porphyrin ring and the imidazole group bound to the Fe atom are described with a standard 6-31G basis set, while the CO subunit includes polarization functions.[35] These calculations yield 500 1D potential energy surfaces, which are then used to parametrize the potential energy surface $W(q_0; \{r_\alpha\})$ as a function of the Cartesian coordinates of all protein atoms $\{r_\alpha\}$. This allows us to construct a model system Hamiltonian written as

$$H(q_0; \{r_\alpha\}) = -\frac{\hbar\omega_0}{2}\frac{\partial^2}{\partial q_0^2} + W(q_0; \{r_\alpha\}) \tag{1}$$

where $\omega_0$ is the CO stretch harmonic frequency. Similar approaches have been employed in other systems, where high-frequency modes are in contact with an environment.[36,37] In order to describe the interaction of the system with external light sources, the projection of the fluctuating dipole moment onto the laser polarization axis, $\mu(q_0;\{r_\alpha\})$, has also been parametrized using the same approach as that for the potential energy surface. The exact forms of the parametrized potential and the dipole moment are given in ref 32. On the basis of an equilibrium MD simulation, one can then evaluate the Hamiltonian and the dipole moment for a large number $M$ of individual pieces of this trajectory, leading to a set of $M$ time-dependent Hamiltonians $H_q(q_0,t) \equiv H(q_0,\{r_\alpha^{(q)}(t)\})$ and dipole functions $\mu_q(q_0,t) \equiv \mu_q(q_0, \{r_\alpha^{(q)}(t)\})$, which become operators that fluctuate in time due to the protein environment. The corresponding dynamics consists of $M$ quantum wave packet propagations $|\psi_q(t)\rangle$, with any observable being calculated by ensemble and orientational averaging. At this level of description, the CO stretch motion is affected by the motion of the porphyrin ring and all of the other atoms of the environment. However, the back reaction, that is, the effect of the highly excited CO stretch onto the motion of the surrounding atoms, is not included.

When interacting with a strong electric field $\mathcal{E}(t)$, the propagation of the wave function includes the matter−field interaction

$$V_q(q_0; t) = -\mu_q(q_0; t)\mathcal{E}(t)\cos\theta_q \tag{2}$$

where for each of the realizations, $\theta_q$ was chosen randomly on the unit sphere to account for an unoriented sample. Simulation of absorption spectroscopy and ladder climbing experiments based on this model have shown to be in good agreement with experiments,[32,38] validating this approach. The averaged populations in the CO stretch levels are thus obtained by

$$P_\nu(t) = \frac{1}{M}\sum_{q=1}^{M} |\langle\phi_q^\nu(t)|\psi_q(t)\rangle|^2 \tag{3}$$

where $|\phi_q^\nu(t)\rangle$ are taken to be the adiabatic eigenfunctions of $H_q(t)$ with eigenenergies $E_q^\nu(t)$.

Local control theory (LCT) consists of the design of external laser fields in order to ensure the increase (or decrease) of a defined observable in time.[10] Here, we apply LCT to minimize the instantaneous energy spread of the quantum system

$$J_{\nu_0}(t) = \frac{1}{M}\sum_{q=1}^{M} \langle\psi_q(t)|(H_q(t) - \bar{\epsilon}_{\nu_0})^2|\psi_q(t)\rangle \tag{4}$$

around the averaged energy of the selected target level $\nu_0$

$$\bar{\epsilon}_{\nu_0} = \frac{1}{M}\sum_{q=1}^{M} E_q^{\nu_0}(t) \tag{5}$$

Because the fluctuations are small compared to the averaged level spacing, as is the case for HbCO, we neglect the explicit time dependence of $H_q(t)$ when calculating the time derivative of $J_{\nu_0}(t)$. Under this assumption, choosing the electric field according to

$$\mathcal{E}_{\nu_0}(t) = \lambda f(t)\frac{1}{M}\sum_{q=1}^{M} \mathrm{Im}\langle\psi_q(t)|(H_q(t) - \bar{\epsilon}_{\nu_0})^2\mu_q(t)|\psi_q(t)\rangle \tag{6}$$

ensures $dJ_{\nu_0}/dt < 0$ at all times if $\lambda f(t) > 0$ and thus induces population transfer to the target state $\nu_0$. Here, $\lambda$ is a scaling factor, which influences the intensity, and $f(t)$ is a window function, which restricts the control pulses to a predefined time interval taken as $f(t) = \exp(-t^2/\tau^2)$ with $\tau = 1$ ps. This procedure has the advantage of being applicable to the complex system at hand; however, the created field may not be the optimal solution.[10]

## RESULTS AND DISCUSSION

In Figure 2, we show as an example the result of a control calculation, where the target state $\nu_0 = 7$ was chosen. With the complicated pulse sequence shown in the middle (Figure 2b), the evolution of the populations in the different vibrational levels as shown in Figure 2c is obtained. The spectrogram (Husimi transformation)[39] showing the instantaneous frequencies (Figure 2a) reveals a structure that is clearly more complicated than a simple chirp. This underlines the necessity of sophisticated pulse shapers that achieve selective excitation. Comparing the frequencies (Figure 2a) with the evolution of the population in the different levels (Figure 2c), one can extract a special excitation mechanism; the pulse starts with a very short,


dx.doi.org/10.1021/jp410473u | J. Phys. Chem. A 2013, 117, 12884−12888

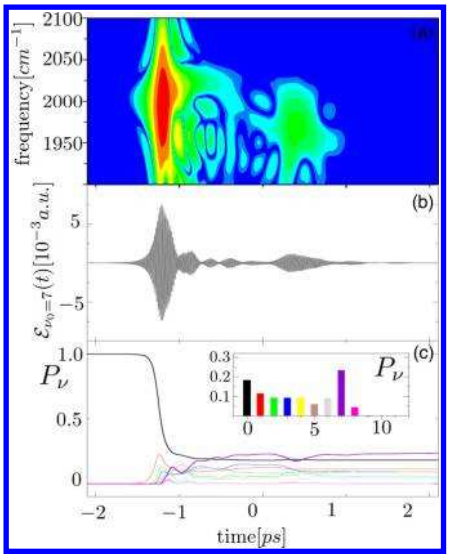


**Figure 2.** Shaped infrared pulse for target level $\nu_0 = 7$ (b) the and corresponding spectrogram (Husimi transformation) (a). Time evolution of populations (c), with the final population distribution shown as an inset.

intense subpulse, which due to the very broad spectral width allows one to populate a large number of vibrational states. The structures following the initial strong pulse (between −1 and 0 ps) induce transitions specifically toward the target state. Interestingly, the small subpulse appearing at around 0.7 ps does not increase the population of the target state but helps to diminish the objective functional by transferring population from $\nu = 3$ to 6 before the envelope function $f(t)$ forces the pulse to stop. After the pulse, we show the final vibrational distributions (Figure 2c, inset). We clearly see that the population in $\nu = \nu_0 = 7$ dominates with respect to the other states. The substantial fraction of the population in the low-lying states stems from the fact that we consider an unoriented molecular sample. Molecules that are unfavorably oriented with respect to the laser polarization axis experience only a weak interaction and thus can only be excited to low-lying states. For an oriented sample, the target state can be populated to almost unity, as described below.

The fact that the field is obtained at every time step by averaging over all realizations (see eq 6) and the neglect of the explicit time dependence of $H_q(t)$ in deriving $\mathcal{E}_{\nu_0}(t)$ leads to pulses that are very similar in structure when compared to those obtained via a dynamics on an averaged surface without fluctuations (see below). As a consequence, the pulses cannot be considered to actively compensate for the fluctuations. Because, for the present system, the fluctuations are small compared to the energy gap, one does not expect a drastic modification of the control scenario when the explicit time dependence of $H_q(t)$ is included. From a principle point of view, however, this is an interesting question that will be addressed in the future.

To systematically asses the probability to excite specific vibrational states, we summarize in Figure 3 the results of a large number of control calculations for target states ranging from $\nu_0 = 1$ to 11. For each target state $\nu_0$, the pulse intensity is scanned by increasing the scaling parameter $\lambda$ up to $3.8 \times 10^4$ au to yield the shown pulse intensities. The effects of the fluctuations and orientational averaging are analyzed by comparing the control scenario based on the full Hamiltonian (Figure 3a) with the orientational averaging suppressed (Figure 3b) and a scenario

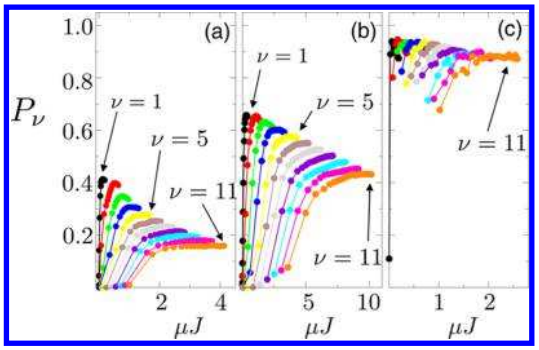


**Figure 3.** Final population distribution after interaction with the LCT pulses and as a function of the total pulse energy (a) when including the protein environment fluctuations and an unoriented sample, (b) when an aligned sample is assumed, and (c) when fluctuations are suppressed and an aligned sample is assumed.

where both the fluctuations and orientational averaging are suppressed (Figure 3c). The elimination of the orientational averaging is achieved by setting $\cos\theta_q = 1$ in eq 2, and the results without fluctuations are based on an averaged potential, obtained using the 500 DFT calculations. Comparing the different panels, we clearly see that for an oriented sample without fluctuations, the different target states can be populated to more than 90% (Figure 3c), while when including fluctuations, this drops significantly (Figure 3b). Considering additionally an unoriented sample leads to a further loss (Figure 3a). This is due to the fraction of molecules oriented unfavorably with respect to the laser polarization axis. Yet, selective population is still possible as is shown in Figure 4. In

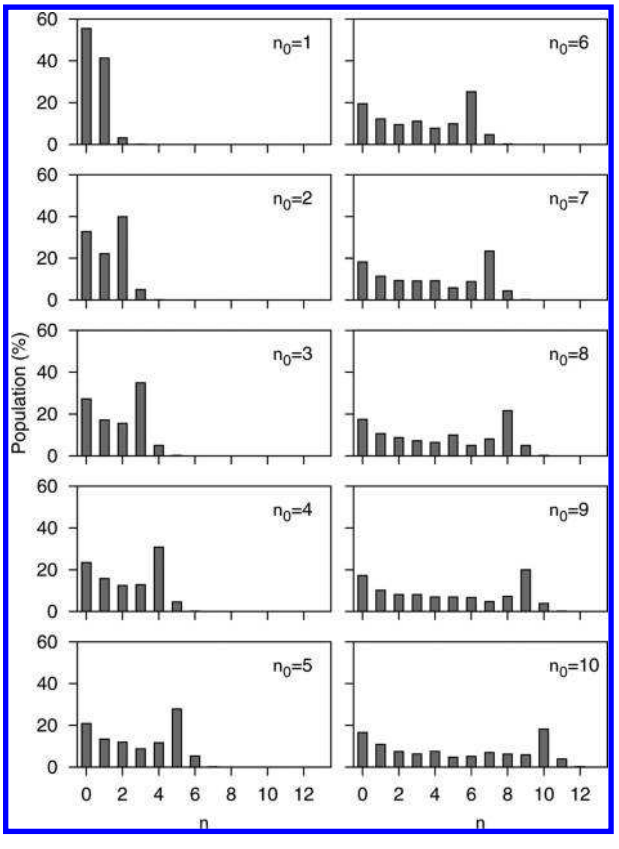


**Figure 4.** Final population distribution for the optimized pulses and for a set of target states $\nu_0$.


dx.doi.org/10.1021/jp410473u | J. Phys. Chem. A 2013, 117, 12884−12888

this figure, we show the results for the targets $\nu_0 = 1, ..., 10$ using their respective optimal pulses (i.e., the maxima of the curves in Figure 3a). Each histogram represents the final population distribution obtained by the optimal pulses for a given $\nu_0$ state target. One can clearly see some population in the nontarget low-lying states due to the orientational averaging, as mentioned above. However, the most striking result is the clear dominating population for each $\nu = \nu_0$ case, indicating that the different pulses indeed lead to a high degree of state-specific excitation to the target level, despite the presence of fluctuations and orientational averaging.

In the remaining part of this article, we show how the significant selective excitation by the control pulse can be detected experimentally. Indeed, transient absorption measurements monitor the population difference in the excited states. This has recently been shown individually in beautiful experimental studies of the Zanni and Joffre groups.[11,23] From the theoretical point of view, the measured spectrum is given by the Fourier transform

$$\sigma(\omega) \approx \int_0^\infty S(t) e^{-i\omega t}\, dt \tag{7}$$

of the correlation function

$$S(t) = \frac{1}{M}\sum_{q=1}^{M} \mathrm{Im}\langle \psi_q(0)|\mu_q(0)U_q(0,t)\mu_q(t)U_q(t,0)|\psi_q(0)\rangle \tag{8}$$

where the time evolution operator $U_q(t,0)$ is written as a function of an ordered exponential

$$U_q(t,0) = T\exp\left(-\frac{i}{\hbar}\int_0^t H_q(\tau)\, d\tau\right) \tag{9}$$

where the time origin $(t = 0)$ is chosen to be immediately after the end of the control pulse and where $\psi_q(0)$ is the system wave function at that time. Following ref 11, the sign of $\sigma(\omega)$ is chosen such that absorption from $\nu \rightarrow \nu + 1$ corresponds to a positive peak, whereas stimulated emission is characterized by a negative peak. Hence, a population inversion between two successive states can be detected by the presence of a negative and a positive peak in the transient signal, as already shown experimentally.[11,22]

Figure 5 summarizes the simulated transient absorption signals when the probe pulse immediately follows the control pulse. As gray lines, we show the averaged target state levels $\bar{\epsilon}_{\nu_0}$ (eq 5). The clear asymmetry of positive and negative peaks centered around $\epsilon_{\nu_0+1} - \epsilon_{\nu 0}$ and $\epsilon_{\nu_0} - \epsilon_{\nu_0-1}$, respectively, (dark gray lines) reflects the successful selective excitation achieved by the preceding shaped mid-IR pulses (cf. Figure 4). The signals are very distinctively centered around $\bar{\epsilon}_{\nu_0}$, not blurred by the remaining populations in the low-lying states. This is due to the fact that the polarizations of the control and the probe pulse are chosen to be parallel. Therefore, the fraction of the population in the lower-lying states, which have not been excited due to an unfavorable orientation, does not contribute to the absorption signal. Similarly, the samples at the edges of the laser focus, where the control is less efficient, do not contribute significantly to the measured signal. Consequently, taking the spatial profile into account does not alter the spectrum drastically. In Figure 5, we superimpose the spectra obtained by neglecting (red lines) or including (blue lines) averaging over a Gaussian laser focus spot size of 20 $\mu$m.[38,40]

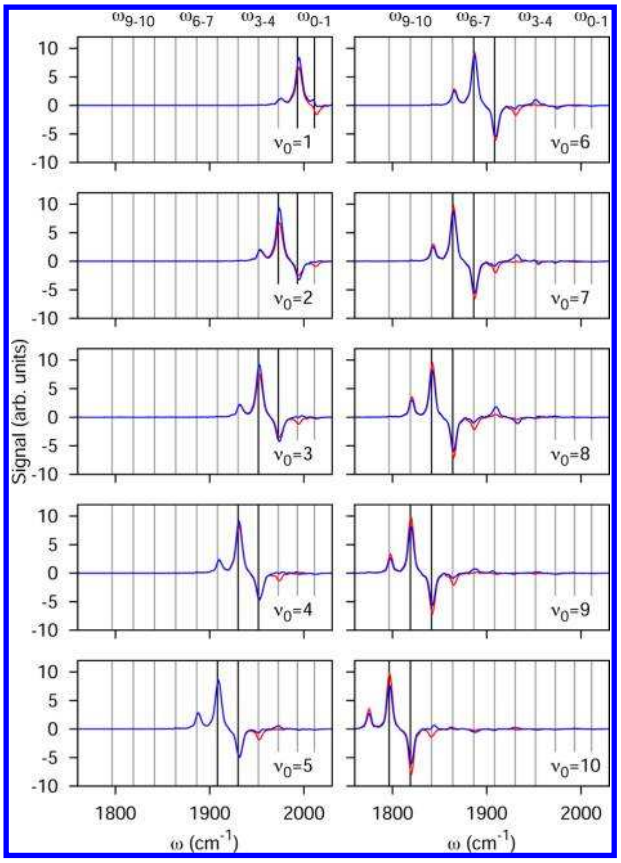


**Figure 5.** (Red) Transient absorption spectrum measured by a weak probe pulse, following the different strong control pulses $\mathcal{E}_{\nu_0}$. Spectra are obtained without spatial averaging (red) and by including spatial averaging over a Gaussian profile of 20 $\mu$m (blue). The transient absorption signal clearly reflects the success of the preceding control.

## CONCLUSION

All of these considerations show that the proposed control–pump scheme is well within experimental feasibility,[11,22] and we hope to stimulate experimental realization in the near future. The presented results show that selective excitation of modes in complex systems is possible through IR pulse shaping, and the created populations are clearly detectable by current transient absorption techniques. By varying the time delay between the control and probe pulse, this should lead to the possibility of direct, state-selective measurements of vibrational relaxation times of states far form equilibrium, bearing the fingerprints of the interaction with the protein environment.

## AUTHOR INFORMATION

### Corresponding Authors

*E-mail: cyril.falvo@u-psud.fr (C.F.).
*E-mail: chris@irsamc.ups-tlse.fr (C.M.).

### Notes

The authors declare no competing financial interest.

## ACKNOWLEDGMENTS

We would like to thank M. Joffre for fruitful discussions. Financial support by the ANR "PROCONTROL" ANR-2011-BS04-027 and the ITN network "FASTQUAST" is gratefully acknowledged. The authors would also like to acknowledge the computational resources provided by CICT (Toulouse).

## REFERENCES


(1) Chergui, M., Ed. *Femtochemistry: Ultrafast Chemical and Physical Processes in Molecular Systems*; World Scientific: Singapore, 1996.

(2) Martin, M. M., Hynes, J. T., Eds. *Femtochemistry and Femtobiology: Ultrafast Events in Molecular Science*; Elsevier: Amsterdam, 2004.

(3) Fecko, C. J.; Eaves, J. D.; Loparo, J. J.; Tokmakoff, A.; Geissler, P. L. Ultrafast Hydrogen-Bond Dynamics in the Infrared Spectroscopy of Water. *Science* **2003**, *301*, 1698−1702.

(4) Cheng, Y.-C.; Fleming, G. R. Dynamics of Light Harvesting in Photosynthesis. *Annu. Rev. Phys. Chem.* **2009**, *60*, 241−262.

(5) Warren, W. S.; Rabitz, H.; Dahleh, M. Coherent Control of Quantum Dynamics — The Dream Is Alive. *Science* **1993**, *259*, 1581−1589.

(6) Gordon, R. J.; Rice, S. A. Active Control of the Dynamics of Atoms and Molecules. *Annu. Rev. Phys. Chem.* **2003**, *48*, 601−641.

(7) Zare, R. N. Laser Control of Chemical Reactions. *Science* **1998**, *279*, 1875−1879.

(8) Rice, S.; Zhao, M. *Optical Control of Molecular Dynamics*; Wiley: New York, 2000.

(9) Shapiro, M.; Brumer, P. *Principles of Quantum Control of Molecular Processes*; Wiley: New York, 2003.

(10) Engel, V.; Meier, C.; Tannor, D. J. Local Control Theory: Recent Applications to Energy and Particle Transfer Processes in Molecules. *Adv. Chem. Phys.* **2009**, *141*, 29−101.

(11) Strasfeld, D. B.; Shim, S.-H.; Zanni, M. T. Controlling Vibrational Excitation with Shaped Mid-IR Pulses. *Phys. Rev. Lett.* **2007**, *99*, 038102.

(12) Strasfeld, D. B.; Shim, S.-H.; Zanni, M. T. New Advances in Mid-IR Pulse Shaping and its Application to 2D IR Spectroscopy and Ground-State Coherent Control. *Adv. Chem. Phys.* **2009**, *141*, 1−28.

(13) Middleton, C. T.; Strasfeld, D. B.; Zanni, M. T. Polarization Shaping in the Mid-IR and Polarization-Based Balanced Heterodyne Detection with Application to 2D IR Spectroscopy. *Opt. Express* **2009**, *17*, 14526−14533.

(14) Maksimenka, R.; Nuernberger, P.; Lee, K. F.; Bonvalet, A.; Milkiewicz, J.; Barta, C.; Klima, M.; Oksenhendler, T.; Tournois, P.; Kaplan, D.; Joffre, M. Direct Mid-Infrared Femtosecond Pulse Shaping with a Calomel Acousto-Optic Programmable Dispersive Filter. *Opt. Lett.* **2010**, *35*, 3565−3567.

(15) Maas, D.; Duncan, D.; Vrijen, R.; van der Zande, W.; Noordam, L. Vibrational Ladder Climbing in NO by (Sub)Picosecond Frequency-Chirped Infrared Laser Pulses. *Chem. Phys. Lett.* **1998**, *290*, 75−80.

(16) Kleiman, V.; Arrivo, S.; Melinger, J.; Heilweil, E. Controlling Condensed-Phase Vibrational Excitation with Tailored Infrared Pulses. *Chem. Phys.* **1998**, *233*, 207−216.

(17) Arrivo, S. M.; Dougherty, T. P.; Grubbs, W. T.; Heilweil, E. J. Ultrafast Infrared Spectroscopy of Vibrational CO-Stretch Up-Pumping and Relaxation Dynamics of $W(CO)_6$. *Chem. Phys. Lett.* **1995**, *235*, 247−254.

(18) Windhorn, L.; Witte, T.; Yeston, J.; Proch, D.; Motzkus, M.; Kompa, K.; Fuss, W. Molecular Dissociation by Mid-IR Femtosecond Pulses. *Chem. Phys. Lett.* **2002**, *357*, 85−90.

(19) Hess, C.; Wolf, M.; Bonn, M. Direct Observation of Vibrational Energy Delocalization on Surfaces: CO on Ru(001). *Phys. Rev. Lett.* **2000**, *85*, 4341−4344.

(20) Witte, T.; Hornung, T.; Windhorn, L.; Proch, D.; de Vivie-Riedle, R.; Motzkus, M.; Kompa, K. Controlling Molecular Ground-State Dissociation by Optimizing Vibrational Ladder Climbing. *J. Chem. Phys.* **2003**, *118*, 2021−2024.

(21) Windhorn, L.; Yeston, J.; Witte, T.; Fuss, W.; Motzkus, M.; Proch, D.; Kompa, K.; Moore, C. Getting Ahead of IVR: A Demonstration of Mid-Infrared Induced Molecular Dissociation on a Sub-Statistical Time Scale. *J. Chem. Phys.* **2003**, *119*, 641−645.

(22) Ventalon, C.; Fraser, J. M.; Vos, M. H.; Alexandrou, A.; Martin, J.-L.; Joffre, M. Coherent Vibrational Climbing in Carboxyhemoglobin. *Proc. Natl. Acad. Sci. U.S.A.* **2004**, *101*, 13216−13220.

(23) Nuernberger, P.; Lee, K. F.; Bonvalet, A.; Bouzhir-Sima, L.; Lambry, J.-C.; Liebl, U.; Joffre, M.; Vos, M. H. Strong Ligand−Protein Interactions Revealed by Ultrafast Infrared Spectroscopy of CO in the Heme Pocket of the Oxygen Sensor FixL. *J. Am. Chem. Soc.* **2011**, *133*, 17110−17113.

(24) Rovira, C.; Schulze, B.; Eichinger, M.; Evanseck, J. D.; Parrinello, M. Influence of the Heme Pocket Conformation on the Structure and Vibrations of the Fe−CO Bond in Myoglobin: A QM/MM Density Functional Study. *Biophys. J.* **2001**, *81*, 435−445.

(25) Merchant, K. A.; Noid, W. G.; Thompson, D. E.; Akiyama, R.; Loring, R. F.; Fayer, M. D. Structural Assignments and Dynamics of the A Substates of MbCO: Spectrally Resolved Vibrational Echo Experiments and Molecular Dynamics Simulations. *J. Phys. Chem. B* **2002**, *107*, 4−7.

(26) Merchant, K. A.; Noid, W. G.; Akiyama, R.; Finkelstein, I. J.; Goun, A.; McClain, B. L.; Loring, R. F.; Fayer, M. D. Myoglobin−CO Substate Structures and Dynamics: Multidimensional Vibrational Echoes and Molecular Dynamics Simulations. *J. Am. Chem. Soc.* **2003**, *125*, 13804−13818.

(27) Bagchi, S.; Thorpe, D. G.; Thorpe, I. F.; Voth, G. A.; Fayer, M. D. Conformational Switching between Protein Substates Studied with 2D IR Vibrational Echo Spectroscopy and Molecular Dynamics Simulations. *J. Phys. Chem. B* **2010**, *114*, 17187−17193.

(28) Zhao, X. J.; Sampath, V.; Caughey, W. S. Infrared Characterization of Nitric Oxide Bonding to Bovine Heart Cytochrome c Oxidase and Myoglobin. *Biochem. Biophys. Res. Commun.* **1994**, *204*, 537−543.

(29) Mayer, E. Freezing-in of Carbonylhemoglobin's CO Conformer Population by Hyperquenching of Its Aqueous Solution into the Glassy State: An FTIR Spectroscopic Study of the Limits of Cryofixation. *J. Am. Chem. Soc.* **1994**, *116*, 10571−10577.

(30) Stock, G. Classical Simulation of Quantum Energy Flow in Biomolecules. *Phys. Rev. Lett.* **2009**, *102*, 118301.

(31) Devereux, M.; Meuwly, M. Force Field Optimization Using Dynamics and Ensemble Averaged Data: Vibrational Spectra and Relaxation in Bound MbCO. *J. Chem. Inf. Model.* **2010**, *50*, 349−357.

(32) Falvo, C.; Meier, C. A Fluctuating Quantum Model of the CO Vibration in Carboxyhemoglobin. *J. Chem. Phys.* **2011**, *134*, 214106.

(33) Frisch, M. J.; Trucks, G. W.; Schlegel, H. B.; Scuseria, G. E.; Robb, M. A.; Cheeseman, J. R.; Montgomery, J. A., Jr.; Vreven, T.; Kudin, K. N.; Burant, J. C.; et al. *Gaussian 03*, revision C.02; Gaussian, Inc.: Wallingford, CT, 2004.

(34) Dolg, M.; Wedig, U.; Stoll, H.; Preuss, H. Energy-Adjusted Ab Initio Pseudopotentials for the First Row Transition Elements. *J. Chem. Phys.* **1987**, *86*, 866−872.

(35) Meier, C.; Heitz, M.-C. Laser Control of Vibrational Excitation in Carboxyhemoglobin: A Quantum Wave Packet Study. *J. Chem. Phys.* **2005**, *123*, 044504.

(36) Li, S.; Schmidt, J. R.; Corcelli, S. A.; Lawrence, C. P.; Skinner, J. L. Approaches for the Calculation of Vibrational Frequencies in Liquids: Comparison to Benchmarks for Azide/Water Clusters. *J. Chem. Phys. 124*, 204110

(37) Meuwly, M. On the Influence of the Local Environment on the CO Stretching Frequencies in Native Myoglobin: Assignment of the B-States in MbCO. *Chem. Phys. Chem.* **2006**, *7*, 2061−2063.

(38) Falvo, C.; Debnath, A.; Meier, C. Vibrational Ladder Climbing in Carboxy-hemoglobin: Effects of the Protein Environment. *J. Chem. Phys.* **2013**, *138*, 145101.

(39) Pearson, B. J.; White, J. L.; Weihnacht, T. C.; Bucksbaum, P. H. Coherent Control Using Adaptive Learning Algorithms. *Phys. Rev. A* **2001**, *63*, 063412.

(40) Nuernberger, P.; Vieille, T.; Ventalon, C.; Joffre, M. Impact of Pulse Polarization on Coherent Vibrational Ladder Climbing Signals. *J. Phys. Chem. B* **2011**, *115*, 5554−5563.